Finite quasiparticle lifetime in disordered superconductors

M. Žemlička, P. Neilinger, M. Trgala, M. Rehák, D. Manca, and M. Grajcar*
Department of Experimental Physics, Comenius University, SK-84248 Bratislava, and Institute of Physics, Slovak Academy of Sciences, Dúbravská cesta, Bratislava, Slovakia

P. Szabó and P. Samuely
Centre of Low Temperature Physics, Institute of Experimental Physics, Slovak Academy of Sciences & Institute of Physics, P. J. Šafárik University, SK-04001 Košice, Slovakia

Š. Gaži
Institute of Electrical Engineering, Slovak Academy of Sciences, Dúbravská cesta, SK-84104 Bratislava, Slovakia

U. Hübner
Leibniz Institute of Photonic Technology, P.O. Box 100239, D-07702 Jena, Germany

V. M. Vinokur
Argonne National Laboratory, 9700 South Cass Avenue, Argonne, Illinois 60439, USA

E. Il'ichev
Leibniz Institute of Photonic Technology, P.O. Box 100239, D-07702 Jena, Germany, and Novosibirsk State Technical University, 20 Karl Marx Avenue, 630092 Novosibirsk, Russia

(Received 19 August 2014; revised manuscript received 27 October 2015; published 8 December 2015)

We investigate the complex conductivity of a highly disordered MoC superconducting film with $k_F l \approx 1$, where k_F is the Fermi wave number and l is the mean free path, derived from experimental transmission characteristics of coplanar waveguide resonators in a wide temperature range below the superconducting transition temperature T_c. We find that the original Mattis-Bardeen model with a finite quasiparticle lifetime, τ, offers a perfect description of the experimentally observed complex conductivity. We show that τ is appreciably reduced by scattering effects. Characteristics of the scattering centers are independently found by scanning tunneling spectroscopy and agree with those determined from the complex conductivity.

DOI: 10.1103/PhysRevB.92.224506 PACS number(s): 74.81.Bd, 74.25.nn, 74.55.+v, 74.78.−w

I. INTRODUCTION

Disordered superconductors are a subject of intense current attention. This interest is motivated not only by the appeal of dealing with the most fundamental issues of condensed matter physics involving interplay of quantum correlations, disorder, quantum and thermal fluctuations, and Coulomb interactions [1–4], but also by the high promise for applications. The existence of states with giant capacitance and inductance in the critical vicinity of the superconductor-insulator transition [2,5] breaks ground for novel microwave engineering exploring duality between phase slips at point-like centers [6] or at phase slip lines [7] and Cooper pair tunneling [8–10]. The feasibility of building a superconducting flux qubit by employing quantum phase slips in a weak link created by highly disordered superconducting wire was demonstrated by Astafiev *et al.* [5]. Yet while there has been notable recent success in describing the dc properties of disordered superconductors [2,9,11], the understanding of their ac response remains insufficient and impedes advancement in their microwave applications.

Recent studies of the electromagnetic response of strongly disordered superconducting films [12,13] revealed a discrepancy between the local density of states measured by scanning tunneling spectroscopy and the density of states, which has been assumed to describe the microwave response. This implies that a model assuming uniform properties of the film fails to describe films near the Ioffe-Regel limit, $k_F l \approx 1$. And although the authors succeeded in explaining the behavior of the imaginary part of the complex conductivity $\sigma_s = \sigma_1 - i\sigma_2$ in a narrow temperature range, the understanding of the real part σ_1, which is mostly influenced by disorder, is far from being complete. Hence a call arises for a simple unified model that can explain both the microwave and the tunneling conductance measurements in strongly disordered superconducting films. In this paper, we discuss a model that meets this challenge and experimentally demonstrate its validity.

II. MOC THIN FILM AND CPW RESONATOR

One of the ways to measure the microwave complex conductivity is to use a coplanar waveguide (CPW) resonator patterned on a thin film of the desired superconductor. The resonator is characterized by two main quantities, the resonant frequency and the quality factor, which can be directly calculated from the complex conductivity. The capacitance of the CPW is explicitly defined by its geometry [14]. The imaginary part of the impedance is mostly represented by the inductance of the CPW, and therefore it determines CPW resonator resonant frequency. The real part of the impedance is determined by the resistive losses in the CPW and therefore

*grajcar@fmph.uniba.sk

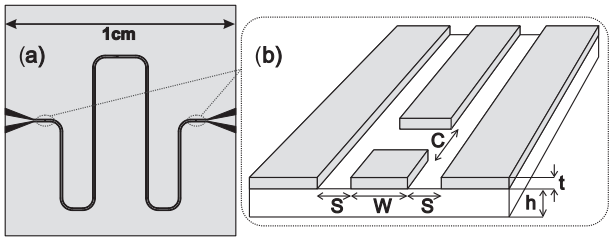

FIG. 1. Scheme of the coplanar waveguide resonator with dimensions W = 50 μm, $S = 30$ μm, C = 10 μm, $t = 10$ nm, and $h = 430$ μm.

influences the internal quality factor [14]. Taking into account the external quality factor Q_{ext} due to input/output coupling capacitances, one can calculate the required loaded quality factor. The structure of the CPW resonator (see Fig. 1) was patterned by optical lithography and argon ion etching of the deposited superconducting thin films. We focused on the study of the properties of disordered 10-nm thin MoC films with sheet resistance $R_\square \approx 180$ Ω [15]. The chosen thickness of 10 nm is optimal for further patterning of superconducting nanostructures which are expected to exhibit quantum phase slips [5]. The films were fabricated by magnetron reactive sputtering, where particles of molybdenum were sputtered from a Mo target onto a sapphire c-cut substrate in an argon-acetylene atmosphere. The partial pressure of acetylene and Ar gas was set to 3×10^{-4} and 5.4×10^{-3} mbar, respectively. The film thickness was controlled by tuning the sputtering time according to the sputtering rate of 10 nm/min. The root mean square (RMS) roughness of the surface, 1 μm × 1 μm, calculated from the AFM topography data was about 0.3 nm. The preparation details are given in Ref. [16].

The transport properties of the MoC thin films were obtained by four-probe measurements. The critical temperatures of the superconducting transition T_c, are very sharp, showing a shift from 8 K for a film thickness $t \geqslant 30$ nm down to 1.3 K for $t = 3$ nm accompanied by an increase in the sheet resistance from several tens of ohms to 1300 Ω, respectively. The transport measurements in magnetic fields as well as the Hall effect measurements allowed us to determine the charge carrier density, the upper critical field, the diffusion coefficient, the coherence length, and the Ioffe-Regel product $k_F l$ in the prepared films. The carrier concentration $n \approx 1.7 \times 10^{23}$ cm^{-3} does not depend on the thickness of the thin film for $t = 15$, 10, and 5 nm, while te sheet resistance $R_\square$ changes considerably, from 110 Ω for $t = 15$ nm, to 200 Ω for $t = 10$ nm, to 1100 Ω for $t = 5$ nm. For thickness $t \approx 10$ nm, $k_F l \approx 2$, indicating that the film is in a highly disordered limit. The details of the transport data analysis will be published elsewhere [17].

III. MICROWAVE MEASUREMENT

Transmission measurements of the CPW resonators yielded temperature dependencies of the resonant angular frequency ω_0 and the quality factor Q, both depending on its complex conductivity. The CPW resonators were designed to have $\omega_0 = 2\pi \times 2.5$ GHz and $Q_{\text{ext}} \approx 4 \times 10^4$ for a conventional superconductor with a large thickness. The design of the resonator was verified by a test resonator fabricated out of a thick MoC film (200 nm, $T_c = 6.7$ K). The measured ω_0

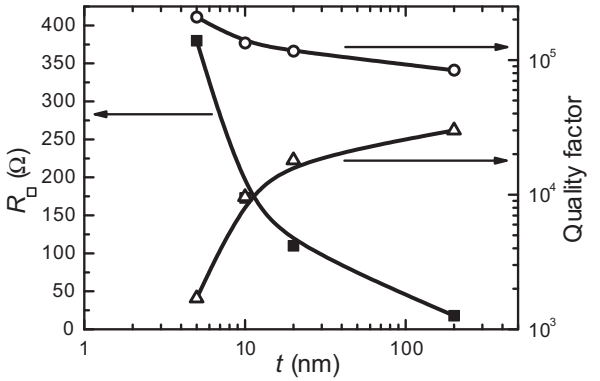

FIG. 2. Thickness dependence of sheet resistances (squares) at temperatures just above T_c and internal quality factors (triangles) of MoC coplanar resonators at temperatures $T \ll T_c$. Internal quality factors, limited by dielectric losses, calculated from the Mattis-Bardeen model for the corresponding $R_\square$ and t (circles) exhibit the opposite trend. Solid lines are guides for the eye.

and Q completely agreed with the design. To compare our experimental data with theory, we calculated the complex impedance of the CPW resonator with known geometry (see Fig. 1) using the complex conductivity given by the Mattis-Bardeen (MB) theory [18].

We measured several MoC samples of different thicknesses (and thus sheet resistances); their parameters are presented in

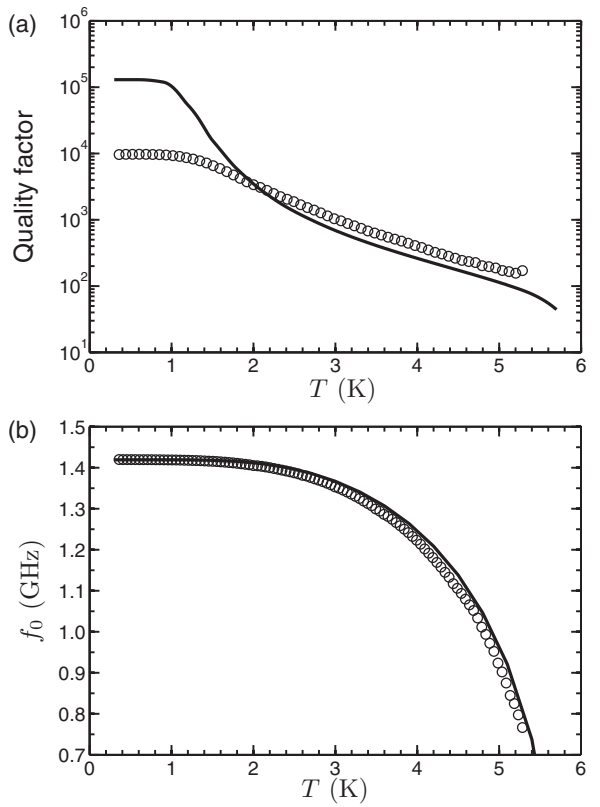

FIG. 3. Temperature dependence of the quality factor Q (a) and the resonant frequency f_0 (b) of the 10-nm thin CPW resonator. Circles are measured data and lines are data calculated from the original Mattis-Bardeen relations ($s \to 0$) for parameters $T_c = 5.8$ K, $R_\square = 180$ Ω, and $\Delta_0 = 1.83 k T_c$.

Fig. 2. The most striking feature of our data is that, while the MB model predicts that with an increase in the sheet resistance the quality factor will increase as well, the experiment reveals the opposite trend: a decrease in the measured quality factors with an increase in the sheet resistance. Furthermore, the measured quality factor noticeably differs from those predicted by the MB model in a wide temperature range [see Fig. 3(a)]. At the same time, the measured resonant frequency falls below the theoretical one [Fig. 3(b)] only slightly, but systematically. This deviation was studied in Ref. [12] for a narrow temperature range.

It is worth noting that including mesoscopic fluctuations, which leads to the broadened superconducting density of states (SDOS) [19], does not noticeably improve the agreement between theory and experiment. It is clear from Fig. 3(a) that the loss of a 10-nm CPW resonator at low temperatures is much higher than predicted by the MB model, explained below.

IV. TUNNELING SPECTROSCOPY

High losses in disordered superconductors imply a finite density of states at Fermi energy. Previous studies of disordered superconductors have shown that both microwave measurements and tunneling spectroscopy indicate a broadened SDOS [13]. Therefore, we have carried out scanning tunneling spectroscopy measurements, making use of a low-temperature scanning tunneling microscope. Figure 4 shows the normalized tunneling conductance spectra obtained between the Au tip and the MoC sample as measured at different temperatures ranging from 0.43 to 5.8 K. Each curve was normalized to the spectrum measured at 5.8 K with the sample in the normal state in order to exclude the influence of the applied voltage on the tunneling barrier and normal density of states of electrodes. Therefore each of these normalized differential conductance versus voltage spectra reflects the SDOS of the MoC sample, smeared by $2k_BT$ in energy at the respective temperature. Consequently, at the low-temperature limit ($k_BT \ll \Delta$), the differential conductance measures the SDOS directly.

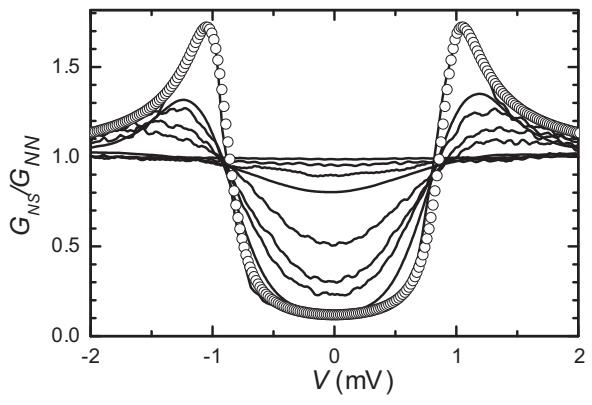

FIG. 4. Temperature dependence of differential tunneling conductance of the 10-nm MoC thin film measured with a scanning tunneling microscope (solid lines). From bottom to top (at zero voltage), data correspond to temperatures $T = 0.43$, 1, 2, 3, 4, 5, 5.4, and 5.6 K. Open circles represent the broadened density of states given by the Dynes formula for $\Gamma = 0.12\Delta_0$, $\Delta_0 = 1.83kT_c$, and $T_c = 5.8$ K.

As evidenced by the 0.43 K curve, the measured SDOS differs from the BCS SDOS: it reveals a significant quasiparticle density of states at the Fermi level and broadened coherence peaks at the gap edges. In our case the best agreement with the experimental data is obtained for the empiric Dynes formula, (3), with parameters $\Gamma = 0.12\Delta_0$, $\Delta_0 = 1.83kT_c$, and $T_c = 5.8$ K. Here we want to emphasize that the experimentally obtained SDOS is broadened but spatially uniform in lateral directions. We have taken scanning tunneling spectroscopy spectra along the 200-nm line and the coefficient of variation of the normalized tunneling conductance at zero voltage and the superconducting energy gap is about 0.05 and 0.025, respectively. There is no characteristic length scale of variations and they can be attributed to the noise and instabilities of the measuring system during long scanning measurements. This is very different from the situation found, for example, in TiN [3], where variations of the superconducting gap are detected by scanning tunneling microscopy (STM) for highly disordered samples. A uniform or "granular" character of the gap distribution in strongly disordered systems could be connected with the fermionic or bosonic scenario of the superconductor-insulator transition and, in MoC films, is the subject of our further research.

V. MODIFICATION OF THE MATTIS-BARDEEN THEORY

Building on the extended BCS theory [20], MB derived the frequency-dependent complex conductivity [18]. To do so, they formally introduced an infinitesimal scattering parameter, $s = 2\pi/\tau$, which was set to 0 at the end of calculations. We may conjecture that in disordered superconductors the finite value of s may acquire the physical meaning of the inverse quasiparticle lifetime and use the corresponding expressions derived in Ref. [21], where both phonon and Coulomb contributions to the quasiparticle lifetime are taken into account. Keeping a finite value of s, as a phenomenological inverse inelastic quasiparticle lifetime, one can derive the modified formulas for the ratio of the superconducting complex conductivity σ_s to the normal conductivity σ_n as

$$\frac{\sigma_s}{\sigma_n} = 1 - \frac{1}{\hbar\omega}\int_{\Delta}^{\infty}[1 - 2f(E)]g(E,\omega)dE, \qquad (1)$$

where $f(E)$ is the Fermi-Dirac distribution function and the propagator g is defined as

$$\begin{aligned} g(E,\omega) &= g_+(E,\omega) - \mathrm{csgn}(E - (\hbar\omega - is))g_-(E,\omega), \\ g_\pm(E,\omega) &= \frac{E}{\sqrt{(E^2-\Delta^2)}}\frac{E \pm \hbar(\omega - is)}{\sqrt{(E \pm \hbar(\omega - is))^2 - \Delta^2}} \\ &\quad + \frac{\Delta}{\sqrt{(E^2-\Delta^2)}}\frac{\Delta}{\sqrt{(E \pm \hbar(\omega - is))^2 - \Delta^2}}. \end{aligned} \qquad (2)$$

Here E is the quasiparticle energy, Δ is the superconducting energy gap, and $\mathrm{csgn}(E - (\omega - is))$ is the complex signum function, defined as $\mathrm{csgn}(z) \equiv 1, -1$, and $\mathrm{sgn}(\Im(z))$ for $\Re(z) > 0$, $\Re(z) < 0$, and $\Re(z) = 0$, respectively. Inspecting Eq. (2), one sees that the first term of $g_\pm(E,\omega)$ is a product of the standard BCS quasiparticle density of states and a similar factor, but with broadened energy states. The broadening can be viewed as the result of Coulomb and/or phonon interactions. It should be noted, however, that the derived propagators

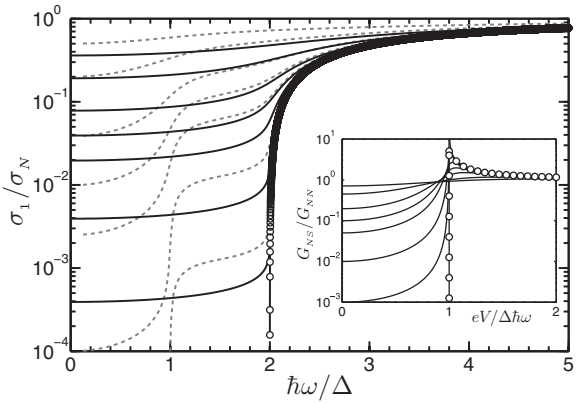

FIG. 5. Frequency dependence of the real part of the superconducting complex conductivity σ_1 for the finite inelastic scattering parameters. Circles represent the original Mattis-Bardeen (MB; scattering parameter $s = 0$). Solid and dashed lines are theoretical curves corresponding, from bottom to top, to the finite values $\hbar s/\Delta$ and $\Gamma/\Delta = 0.001$, 0.01, 0.05, 0.1, 0.2, 0.5, and 1 for the Nam and MB models with finite scattering, respectively. Inset: Normalized tunneling conductance of the normal metal-insulator-superconductor tunnel junction for the same values of $\Gamma = \hbar s$.

$g_{\pm}(E,\omega)$ include the same broadened density of states as described by the empiric Dynes formula used in tunneling and point contact spectroscopy [22,23],

$$N(E) = \Re\left\{\mathrm{sgn}(E)\frac{E+i\Gamma}{\sqrt{(E+i\Gamma)^2-\Delta^2}}\right\}, \tag{3}$$

with the inelastic scattering parameter $\Gamma = \hbar s$. The superconducting complex conductivity and the tunneling conductance for finite inelastic scattering parameters are shown in Figs. 5 and 6. Although the MB model with finite scattering provides results consistent with microwave measurements, the results contain a product of the BCS and broadened SDOS, which seems to be nonphysical. Nevertheless, one can include the

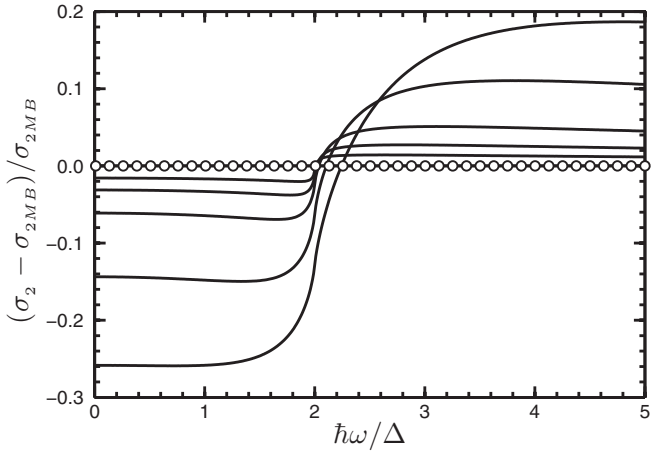

FIG. 6. Relative deviation of the imaginary part of the superconducting complex conductivity σ_2 from the original Mattis-Bardeen theory (circles) for the same values of parameter $\hbar s$ as in Fig. 5. Increasing the parameter s decreases the magnitude of the σ_2 values for frequencies below 2Δ.

broadened density of states in the Nam model [24] elaborated for superconductors containing magnetic impurities. Nam generalized the MB model for arbitrary complex functions $n(E)$ and $p(E)$, whose real parts correspond to the densities of states and Cooper pairs, respectively. For the Dynes broadened density of states, the complex functions $n(E)$ and $p(E)$ can be defined as

$$\begin{aligned} n(E) &\equiv \mathrm{sgn}(E)\frac{E+i\Gamma}{\sqrt{(E+i\Gamma)^2-\Delta^2}}, \\ p(E) &\equiv \mathrm{sgn}(E)\frac{\Delta}{\sqrt{(E+i\Gamma)^2-\Delta^2}}, \end{aligned} \tag{4}$$

and the normalized superconducting complex conductivity reads

$$\begin{aligned} \frac{\sigma_1}{\sigma_n} &= \frac{1}{\hbar\omega}\int_{-\infty}^{\infty}[f(E)-f(E+\hbar\omega)][\Re(n(E))\Re(n(E+\hbar\omega)) \\ &\quad +\Re(p(E))\Re(p(E+\hbar\omega))]dE, \\ \frac{\sigma_2}{\sigma_n} &= \frac{1}{\hbar\omega}\int_{-\infty}^{\infty}[1-2f(E+\hbar\omega)][\Im(n(E))\Re(n(E+\hbar\omega)) \\ &\quad +\Im(p(E))\Re(p(E+\hbar\omega))]dE. \end{aligned} \tag{5}$$

The square roots are taken to mean the principal square root with real part $\geqslant 0$.

The real parts of the complex conductivity calculated for the Nam model and the modified MB model with finite scattering are compared with those for the standard MB model in Fig. 5. Both models result in an increase in the real part of the complex conductivity in comparison to the standard MB model. At frequencies $\omega > 2\Delta$ this increase is almost indistinguishable, whereas at frequencies $\omega < 2\Delta$ the difference is significant. The difference is the most noticeable at $\omega = \Delta$, where the Nam model exhibits a peculiarity. The resonant frequency of our resonator is much lower than the energy gap $\omega \ll \Delta$, therefore we cannot test the peculiarity at $\omega \approx \Delta$ directly. The terahertz (THz) spectroscopy performed recently on NbN samples [25] could detect this peculiarity but measurement temperatures are too high to resolve it.

In order to avoid problems with normalization and geometrical factor inaccuracy it is convenient to compare theoretical and experimental results via the ratio σ_2/σ_1. Since the geometrical factors of the resonator are canceled out, this ratio can be expressed as a function of the resonant frequency and the quality factor of the CPW resonator:

$$\frac{\sigma_2}{\sigma_1} = Q\left(1-\left(\frac{\omega_0}{\omega_g}\right)^2\right). \tag{6}$$

Here ω_g is the resonant frequency of the resonator in the normal state of a lossless metal. In Fig. 7 we compare the experimental data with the σ_2/σ_1 temperature dependence calculated for different values of the parameters s and Γ corresponding to the MB and Nam models, respectively.

At high temperatures, $T > T_c/2$, small values of the scattering parameter provide a fair agreement between the experimental data and the prediction by the standard MB theory; i.e., this theory works well. However, at very low temperatures a larger scattering parameter is required to fit the measured data, and it is not possible to find any intermediate

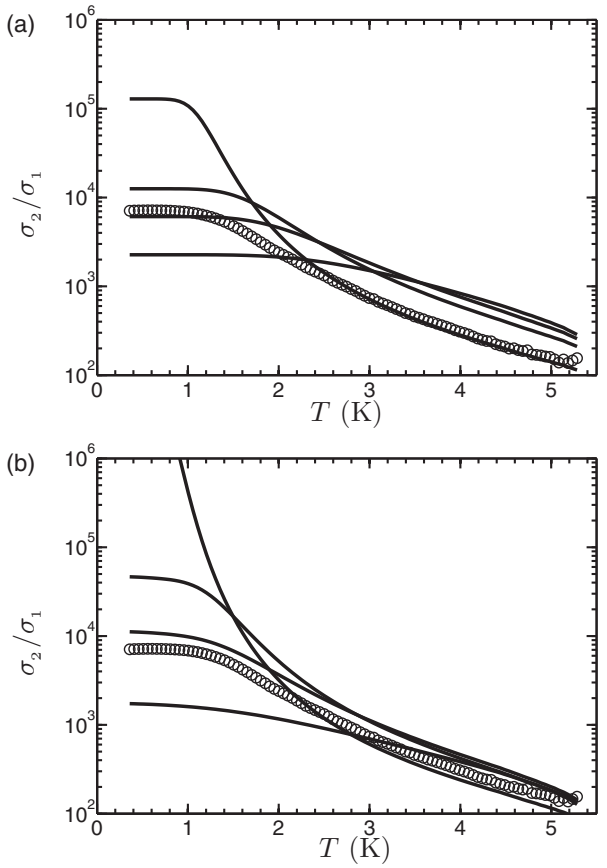

FIG. 7. Measured ratio σ_2/σ_1 (open circles) for the 10-nm thin MoC CPW resonator compared with the ratio calculated (a) from the Mattis-Bardeen relations with finite inelastic scattering and (b) from the Nam model for various values of the parameters s and Γ, respectively. At low temperatures (below 1 K) the lines, from top to bottom, correspond to $\hbar s/\Delta_0$ and $\Gamma/\Delta_0 = 0.01$, 0.1, 0.2, and 0.5.

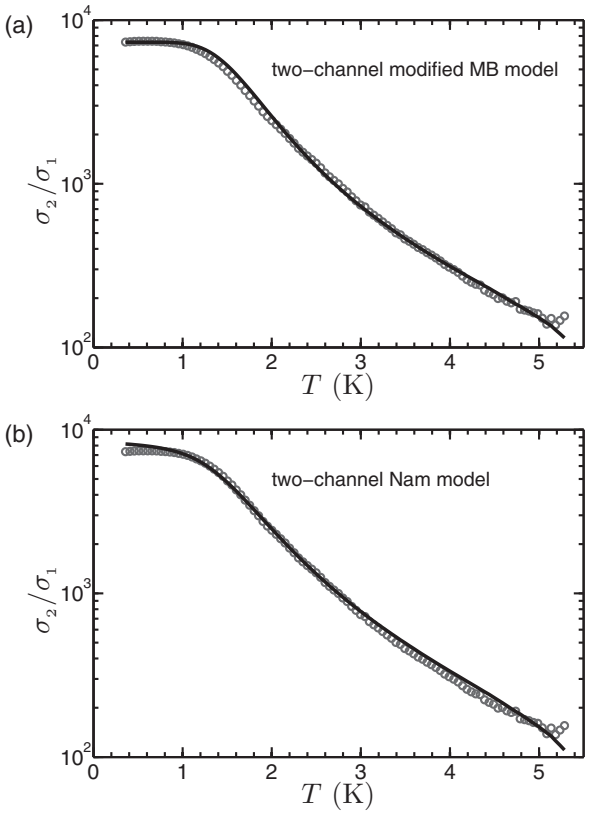

FIG. 8. Temperature dependence of the ratio σ_2/σ_1 of the 10-nm thin CPW resonator. Circles are measured data fitted by the two-channel model with (a) modified Mattis-Bardeen relations (solid line) for parameters $\kappa = 0.34$, $\Delta_0 = 1.83kT_c$, $T_c = 5.7$ K, $\hbar s_s = 0.24\Delta_0$, and $s_b = 0$ and (b) Nam relations (solid line) for parameters $\kappa = 0.10$, $\Delta_0 = 1.83kT_c$, $T_c = 5.7$ K, and $\Gamma = 0.25\Delta_0$.

value of s or Γ to obtain a reasonable agreement with both tunneling and microwave experiments for the complete temperature range.

VI. TWO-CHANNEL MODELS

The MB model with finite scattering parameter s provides a hint about how to solve the problem. In order to obtain a self-consistent picture, one should include also a "channel" corresponding to the photon scattering from the BCS to the BCS density of states which corresponds to the standard MB model with $s \to 0$. Hence let us adopt a two-channel model in which the total complex conductivity is the weighted sum of two contributions $\sigma = (1-\kappa)\sigma_b + \kappa\sigma_s$, where the σ_s corresponds to the channel with enhanced scattering s_s taken as the fitting parameter, while the chanel without scattering (bulk channel) s_b is taken to be 0 and the parameter $\kappa \in \langle 0,1\rangle$ is the filling factor. Surprisingly, the modified MB model with a weighted sum of two contributions gives excellent agreement with experimental results [see Fig. 8(a)]. Here we can conclude that in order to fit the complex conductivity and tunneling conductivity of disordered superconductors for a similar set of parameters, one should apply the two-channel model. A similar two-channel model was used by Sherman *et al.* in Ref. [25], where the authors should have included an excess conductivity in order to fit their experimental data measured at a much higher range of frequencies than in the current work. The same procedure was applied to the Nam model and the results are shown in Fig. 8(b). The results are satisfactory for temperatures above $T_c/2$, but the qualitative agreement between theory and experiment for low temperatures is much worse than that for the modified MB model.

Remarkably, if we adopt the argument of Sherman *et al.* [26] that the upper metallic electrode used for tunneling spectroscopy measurements can screen Coulomb interactions, which can, in turn, increase the measured energy gap, it is not necessary to fit the complex conductivity for the same values of the energy gap as measured by tunneling spectroscopy. Hence, the Δ_0 can be taken as a fitting parameter, and a value smaller than the one obtained with tunneling spectroscopy is expected. The best fit of the complex conductivity was obtained for $\kappa \to 0$, which is in fact a single-channel model. The suppressed gap obtained is $\Delta_0 \approx 1.5kT_c$, which is much smaller than the $\Delta_0 \approx 1.83kT_c$ measured by STM, whereas the scattering parameter, $\Gamma \approx 0.13\Delta_0$, is very close to the value obtained by STM [see Fig. 9(a)]. Interestingly, for the Nam theory the same approach, with a single channel and suppressed Δ_0, does not change the results in comparison with

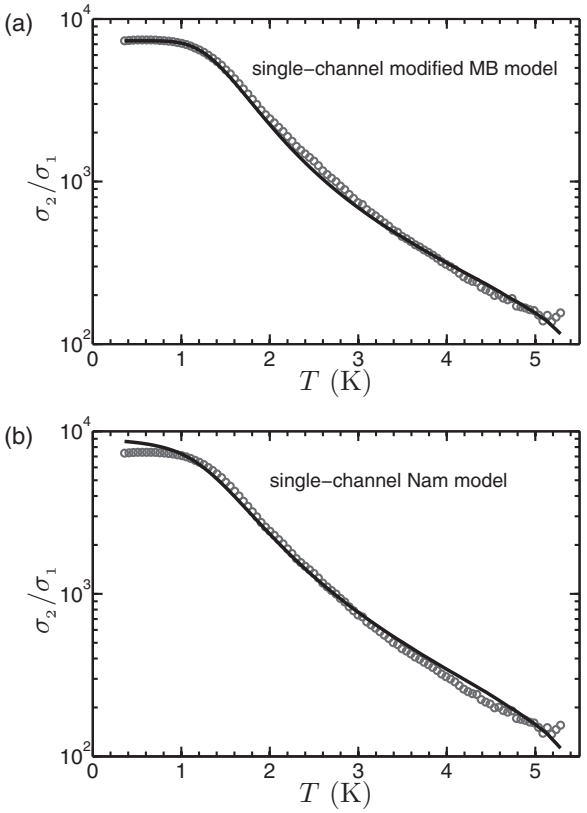

FIG. 9. Same experimental data as in Fig. 8 (circles) fitted by the single-channel model with (a) modified Mattis-Bardeen relations (solid line) for parameters $\Delta_0 = 1.5kT_c$, $T_c = 5.7$ K, and $\hbar s = 0.13\Delta_0$ and (b) Nam relations (solid line) for parameters $\Delta_0 = 1.7kT_c$, $T_c = 5.7$ K, and $\Gamma = 0.23\Delta_0$.

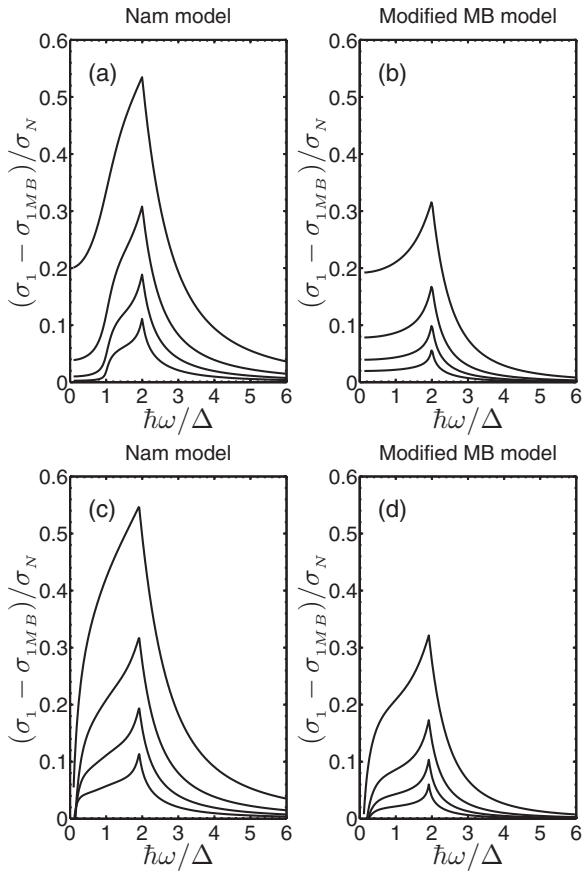

FIG. 10. Normalized deviation of the real part of the complex conductivity σ_1 to the standard Mattis-Bardeen (MB) counterpart ($s = 0$) for the Nam (a, c) and the modified MB (b, d) models for temperatures $T = 0$ (a, b) and $T = 0.4T_c$ (c, d). From bottom to top, the curves in each graph correspond to inelastic scattering parameters Γ/Δ_0 and $\hbar s/\Delta_0 = 0.05$, 0.1, 0.2, and 0.5.

the two-channel model [see Fig. 9(b)]. For both single-channel models the ratio Δ/kT_c is below the BCS universal value, 1.76.

Nevertheless, in both cases, single and two channel, considerable inelastic scattering is required, which fully justifies the concept of a finite quasiparticle lifetime in disordered superconductors. Surprisingly, the Nam models do not fit the experimental data as well as the modified MB models. Therefore, it would be interesting to check both models experimentally at $\omega \approx \Delta/\hbar$, where they exhibit the most remarkable difference. THz spectroscopy can provide such experimental data.

In Ref. [25], THz spectroscopy reveals a deviation of the measured real part of the complex conductivity σ_1 from the standard MB counterpart. The difference, which the authors ascribe to a contribution of broken symmetry in disordered superconductors, is compared with the Higgs model [27]. However the deviations presented in Fig. 3 in Ref. [25] can be even better described by models with a broadened density of states. For example, the position of the peaks clearly changes with the energy gap of the samples and there is no cutoff frequency at which the deviation of the measured real part of the complex conductivity from the standard MB model $\sigma_1 - \sigma_{1\mathrm{MB}}$ saturates to 0. Both features are present in Fig. 10, where the deviation of the theoretical curves $\sigma_1(\omega)$ from the standard MB model ($s = 0$) are shown for various inelastic scattering parameters. These results show that one should take into account the broadened density of states in the MB model and more exotic models should be compared to the modified MB model.

Our two-channel model is phenomenological and does not address the problem of the microscopic origin of the second channel with enhanced inelastic scattering. Nevertheless, the Dynes empiric formula for the broadened density of states, introduced in 1984 for disordered superconductors [22], is present in the MB model, and MB obtained it already in 1958. Such a broadened density of states was observed in many superconducting systems such as disordered superconductors [22], high-T_c superconductors [23], MgB_2 [28], and iron-based superconductors [29]. It seems that, for some paths, the scattering parameter s is not renormalized to 0 and the MB model with finite scattering rate s is a good first approximation. The scattering is probably caused by two-level systems located very homogeneously at the MoC-sapphire interface, which are present even if special precautions are made [30]. This hypothesis is corroborated by our STM/scanning tunneling spectroscopy, which reveal the same inelastic scattering parameter Γ even for atomically flat surfaces with no adsorbed impurity.

VII. CONCLUSION

In conclusion, the two-channel model well describes both microwave and tunneling conductance measurements over a wide temperature range: from 300 mK up to almost T_c. The enhanced scattering channel dominates at low temperatures, which is consistent with the low-temperature losses in high-quality CPW resonators made of conventional superconductors [30,31], where the quality factor is limited by the interface scattering. However, if STM provides an overestimated value of the superconducting energy gap, the results can even be described by the single-channel model with enhanced scattering. In disordered superconducting films such scattering leads to the suppression of electron diffusion and, accordingly, to enhancement of the Coulomb interaction [32,33]. This is consistent with the rapid decrease in the quality factors for thinner superconducting films as shown in Fig. 2.

The main features shown in MoC disordered superconductors apply also for other disordered superconductors, such as NbN and TiN [13,25]. For example, the deviation of the real part of the complex conductivity σ_1 from the standard MB one ($s = 0$), measured in Ref. [25], can be well explained by finite inelastic scattering as shown in Fig. 10, providing even better agreement with experiment. Thus, the original MB model with finite inelastic scattering or the Nam model is able to describe microwave and tunneling experiments in disordered superconductors, while more advanced models are failing. Our results providing a simple expression for the complex conductivity call for further theoretical, as well as experimental, research aimed at clarifying what the simple MB theory with finite inelastic scattering captures that is lost in more advanced machineries.

ACKNOWLEDGMENTS

This work was supported by the European Community's Seventh Framework Programme (FP7/2007-2013) under Grant No. 270843 (iQIT), by the MP-1201 COST Action, by the Slovak Research and Development Agency under the Contract Nos. DO7RP003211, APVV-0515-10, APVV-0036-11, APVV-0088-12, APVV-14-0605, VEGA 2/0135/13 and VEGA 1/0409/15 and by the U.S. Department of Energy, Office of Science, Materials Sciences and Engineering Division. E.I. acknowledges partial support from Russian Ministry of Science and Education Contract No. 8.337.2014/K.

[1] W. Escoffier, C. Chapelier, N. Hadacek, and J.-C. Villégier, Phys. Rev. Lett. **93**, 217005 (2004).
[2] V. M. Vinokur, T. I. Baturina, M. V. Fistul, A. Y. Mironov, M. R. Baklanov, and C. Strunk, Nature **452**, 613 (2008).
[3] B. Sacépé, C. Chapelier, T. I. Baturina, V. M. Vinokur, M. R. Baklanov, and M. Sanquer, Phys. Rev. Lett. **101**, 157006 (2008).
[4] A. D. Zaikin, D. S. Golubev, A. van Otterlo, and G. T. Zimányi, Phys. Rev. Lett. **78**, 1552 (1997).
[5] O. V. Astafiev, L. B. Ioffe, S. Kafanov, Y. A. Pashkin, K. Y. Arutyunov, D. Shahar, O. Cohen, and J. S. Tsai, Nature **484**, 355 (2012).
[6] M. Tinkham, *Introduction to Superconductivity*, 2nd ed. (McGraw–Hill, New York, 1996).
[7] E. Il'ichev, V. Kuznetsov, and V. Tulin, Pis'ma Zh. Eksp. Teor. Fiz. **56**, 297 (1992) [JETP Lett. **56**, 295 (1992)].
[8] J. E. Mooij and Y. V. Nazarov, Nat. Phys. **2**, 169 (2006).
[9] T. I. Baturina and V. M. Vinokur, Ann. Phys. **331**, 236 (2013).
[10] T. I. Baturina, D. Kalok, A. Bilui, V. M. Vinokur, M. R. Baklanov, A. K. Gutakovskii, A. V. Latyshev, and C. Strunk, Appl. Phys. Lett. **102**, 042601 (2013).
[11] A. M. Goldman, Int. J. Mod. Phys. **24**, 4081 (2010).
[12] E. F. C. Driessen, P. C. J. J. Coumou, R. R. Tromp, P. J. de Visser, and T. M. Klapwijk, Phys. Rev. Lett. **109**, 107003 (2012).
[13] P. C. J. J. Coumou, E. F. C. Driessen, J. Bueno, C. Chapelier, and T. M. Klapwijk, Phys. Rev. B **88**, 180505 (2013).
[14] M. Göppl, A. Fragner, M. Baur, R. Bianchetti, S. Filipp, J. M. Fink, P. J. Leek, G. Puebla, L. Steffen, and A. Wallraff, J. Appl. Phys. **104**, 113904 (2008).
[15] S. J. Lee and J. B. Ketterson, Phys. Rev. Lett. **64**, 3078 (1990).
[16] M. Trgala, M. Žemlička, P. Neilinger, M. Rehák, M. Leporis, Š. Gaži, J. Greguš, T. Plecenik, T. Roch, E. Dobročka, and M. Grajcar, Appl. Surface Sci. **312**, 216 (2014).
[17] J. Kačmarčík *et al.* (unpublished).
[18] D. C. Mattis and J. Bardeen, Phys. Rev. **111**, 412 (1958).
[19] M. V. Feigel'man and M. A. Skvortsov, Phys. Rev. Lett. **109**, 147002 (2012).
[20] J. Bardeen, L. N. Cooper, and J. R. Schrieffer, Phys. Rev. **108**, 1175 (1957).
[21] T. P. Devereaux and D. Belitz, Phys. Rev. B **44**, 4587 (1991).
[22] R. C. Dynes, J. P. Garno, G. B. Hertel, and T. P. Orlando, Phys. Rev. Lett. **53**, 2437 (1984).
[23] A. Plecenik, M. Grajcar, Š. Beňačka, P. Seidel, and A. Pfuch, Phys. Rev. B **49**, 10016 (1994).
[24] S. B. Nam, Phys. Rev. **156**, 470 (1967).
[25] D. Sherman, U. S. Pracht, B. Gorshunov, S. Poran, J. Jesudasan, M. Chand, P. Raychaudhuri, M. Swanson, N. Trivedi, A. Auerbach, M. Scheffler, A. Frydman, and M. Dressel, Nat. Phys. **11**, 188 (2015).
[26] D. Sherman, B. Gorshunov, S. Poran, N. Trivedi, E. Farber, M. Dressel, and A. Frydman, Phys. Rev. B **89**, 035149 (2014).
[27] M. Swanson, Y. L. Loh, M. Randeria, and N. Trivedi, Phys. Rev. X **4**, 021007 (2014).
[28] G. Karapetrov, M. Iavarone, W. K. Kwok, G. W. Crabtree, and D. G. Hinks, Phys. Rev. Lett. **86**, 4374 (2001).
[29] P. Szabó, Z. Pribulová, G. Pristáš, S. L. Bud'ko, P. C. Canfield, and P. Samuely, Phys. Rev. B **79**, 012503 (2009).
[30] A. Bruno, G. de Lange, S. Asaad, K. L. van der Enden, N. K. Langford, and L. DiCarlo, Appl. Phys. Lett. **106**, 182601 (2015).
[31] P. Macha, S. H. W. van der Ploeg, G. Oelsner, E. Il'ichev, H.-G. Meyer, S. Wünsch, and M. Siegel, Appl. Phys. Lett. **96**, 062503 (2010).
[32] A. M. Finkel'shtein, Pis'ma Zh. Eksp. Teor. Fiz. **45**, 37 (1987) [JETP Lett. **45**, 46 (1987)].
[33] A. M. Finkel'shtein, Physica B: Condens. Matter **197**, 636 (1994).